RSC Advances

PAPER

View Article Online
View Journal | View Issue

Cite this: *RSC Adv.*, 2020, **10**, 28975

Microenvironmental topographic cues influence migration dynamics of nasopharyngeal carcinoma cells from tumour spheroids†

Bowie P. Lam,[ab] Sarah K. C. Cheung,[bc] Yun W. Lam[bc] and Stella W. Pang *[ab]

Tumour metastasis is a complex process that strongly influences the prognosis and treatment of cancer. Apart from intracellular factors, recent studies have indicated that metastasis also depends on microenvironmental factors such as the biochemical, mechanical and topographical properties of the surrounding extracellular matrix (ECM) of tumours. In this study, as a proof of concept, we conducted tumour spheroid dissemination assay on engineered surfaces with micrograting patterns. Nasopharyngeal spheroids were generated by the 3D culture of nasopharyngeal carcinoma (NPC43) cells, a newly established cell line that maintains a high level of Epstein–Barr virus, a hallmark of NPC. Three types of collagen I-coated polydimethylsiloxane (PDMS) substrates were used, with 15 μm deep "trenches" that grated the surfaces: (a) 40/10 μm ridges (R)/trenches (T), (b) 18/18 μm (R/T) and (c) 50/50 μm (R/T). The dimensions of these patterns were designed to test how various topographical cues, different with respect to the size of tumour spheroids and individual NPC43 cells, might affect dissemination behaviours. Spreading efficiencies on all three patterned surfaces, especially 18/18 μm (R/T), were lower than that on flat PDMS surface. The outspreading cell sheets on flat and 40/10 μm (R/T) surfaces were relatively symmetrical but appeared ellipsoid and aligned with the main axes of the 18/18 μm (R/T) and 50/50 μm (R/T) grating platforms. Focal adhesions (FAs) were found to preferentially formed on the ridges of all patterns. The number of FAs per spheroid was strongly influenced by the grating pattern, with the least FAs on the 40/10 μm (R/T) and the most on the 50/50 μm (R/T) substrate. Taken together, these data indicate a previously unknown effect of surface topography on the efficiency and directionality of cancer cell spreading from tumour spheroids, suggesting that topography, like ECM biochemistry and stiffness, can influence the migration dynamics in 3D cell culture models.

Received 26th April 2020
Accepted 22nd July 2020

DOI: 10.1039/d0ra03740k

rsc.li/rsc-advances

1. Introduction

Cancer metastasis is the major cause of patient morbidity and mortality. The complex process of tumour metastasis involves the migration of tumour cells from a primary site to distant organs *via* the blood circulation and/or lymphatics system of the body.[1] When tumour cells undergo epithelial mesenchymal transition, they acquire metastatic properties enhancing cell mobility, extracellular matrix (ECM) invasion potential and resistance to apoptotic stimuli.[2] As a result, therapeutic interventions targeting cancer metastasis has become a major focus of cancer research in recent decades.[3]

Tumour metastasis is influenced by a combination of biochemical and physical cues in the surrounding microenvironment.[4] Many model systems have been established to mimic the physical tumour environment and study how the architectural information of the extracellular milieu controls cancer cell migration. We and others have demonstrated that, whereas cells move randomly on flat surfaces, their motility and directionality could be guided by topographical patterns on engineered surfaces[5–9] and microchannels.[10] It is likely that cancer cells interpret specific topographical signals through focal adhesion (FA) maturation and cytoskeletal organisation, which in turn generates anisotropic forces that control cell migration.[8,11] Interestingly, cells respond to microenvironmental topography differently depending on their transformation status. For example, cancer cells in monolayered culture have been shown to trespass vertical boundaries on the substratum, while non-cancerous cells could not.[12] Grating platforms with zigzag patterns can even control the migration direction of cells depending on their metastatic status.[13]

These discoveries indicate that simple patterned surfaces can provide a versatile model system for the *in vitro*

[a]*Department of Electrical Engineering, City University of Hong Kong, Hong Kong. E-mail: pang@cityu.edu.hk*

[b]*Centre for Biosystems, Neuroscience, and Nanotechnology, City University of Hong Kong, Hong Kong*

[c]*Department of Chemistry, City University of Hong Kong, Hong Kong*

† Electronic supplementary information (ESI) available. See DOI: 10.1039/d0ra03740k

characterisation of the roles of microenvironmental cues on cancer cell migration and spreading. However, most of the studies in this research field utilised two-dimensional (2D) adherent cells, which did not provide a physiologically relevant picture of cancer cell metastasis. Three-dimensional (3D) tumour spheroids are frequently employed as a more clinically relevant *in vitro* cell culture model of cancer cells.[9] There are many different experimental techniques to generate tumour spheroids for *in vitro* cancer studies.[14] One of the common ways to generate tumour spheroids for *in vitro* cancer studies is the use of ultra-low attachment plate together with hydrogels consist of ECM.[13] Tumour spheroids mimic the *in vivo* tumour mass with an outer layer of proliferating cells and a central core of hypoxic cells.[9] These spheroid cells exhibit stem-cell like properties, and they are resistance to chemotherapeutic drugs.[9] Moreover, the outgrowth of cancer cells from tumour spheroids into the surroundings, either in the form of a 2D surface,[15] 3D gel matrix[16] or membrane filter,[17] have been used as a convenient *in vitro* model for studying the mechanism of cell invasiveness and screening anti-metastasis compounds. For example, glioblastoma spheroids, generated from the culture of U-87MG and KNS42 cells in gelatin-coated flat-bottomed wells, have been observed to disseminate when transferred to a flat substrate.[18] Individual cells rapidly invade radially from the spheroids with locomotory dynamics characteristic of the metastasis status of each cell line. Using tumour spheroids, many researchers have studied the roles of tumour microenvironment in the spreading characteristics of 3D cultured cancer cells.[19,20] For example, a previous study introduced two-photon laser to create 3D microtunnels in collagen, in which the entire mouse mammary tumor spheroids were entrapped, and observed the deformation of the microtunnel during the subsequent cell invasion.[21] Meanwhile, the dissemination of epithelial ovarian cancer cells from tumour spheroids have been shown to be strongly influenced by substrate rigidity, possibly involving ROCK and FAK pathways.[22] This suggests that the interplay of the interaction of ECM remodeling and the mechanical properties of tumour microenvironment can exercise important controls over metastasis. However, the roles of other physical signals, such as tissue topography, in tumour dissemination remain unexplored.

In our previous work, the investigation of nasopharyngeal epithelial (NP460) and nasopharyngeal carcinoma (NPC43) single cell migration speed, orientation, and morphology on grating platforms with different dimensions of 5/5, 18/18, and 50/50 μm ridges (R)/trenches (T) was reported.[4] However, cells in our bodies tend to cluster together and interact with their local microenvironment in reality. Cancer cells often group together and grow continuously to develop tumors,[23] with epithelial cells and other elements in the ECM to form spheroids.[24] For collective cell migration, many factors such as cell density and strength of cell–cell adhesions also affect the response of cells to the extracellular environment.[25] Therefore, it is important to investigate the migration behaviours of NPC43 cells from spheroids. This study reports, for the first time, the effect of microenvironmental topography on the dynamics of cell spreading of tumour spheroids. As a proof of concept, we focused our study on nasopharyngeal carcinoma (NPC), one of the most common malignancies in southern China and Southeast Asia.[26] It is highly invasive and metastatic.[19] NPC is a very complex disease which is poorly understood on the molecular genetic level. Therefore, effective therapeutic interventions targeting cancer metastasis are urgently needed. However, as NPC originates from the nasopharynx, which is structurally distinct from that in rodents,[27] the establishment of orthotropic animal models is technically challenging[28] and most *in vivo* studies on NPC are based on subcutaneous xenografts which do not necessarily recapitulate the human disease. The lack of physiologically relevant *in vivo* NPC models makes the development of cell culture models a priority for the study of NPC pathology and therapy. In this study, we investigate the metastasis characteristics of NPC tumour spheroid cells on engineered patterned substrates. This study will shed lights on the impact of topographic cues on 3D NPC spheroid cells *in vitro*.

2. Material and methods

2.1 Cell culture

An EBV+ nasopharyngeal cell line (NPC43)[20] was used in this study. NPC43 cells, stably expressing Lifeact-mCherry,[4] were cultured in RPMI medium 1640 (1X, Gibco) supplemented with 10% fetal bovine serum, 1% antibiotic antimycotic (Gibco; 100 units per ml penicillin G sodium, 100 mg ml^{-1} of streptomycin, and 0.25 mg ml^{-1} of amphotericin B), and 0.2% 2 mM rock inhibitor Y-27,632 (ENZO) at 37 °C in a 5% CO_2. NPC43 cells were maintained in 2D culture, passaged every 3 days in 1 : 3 ratio until 80% confluence. Cells cultured for more than 20 passages were discarded. To generate NPC tumour spheroids, NPC43 cells were harvested by trypsinization and resuspended in ice-cold tumour spheroid medium (cell culture medium containing 2% (v/v) Matrigel (CORNING, cat no. 354270)) at a concentration of 10^6 cells per ml. 100 μl of the cell suspension was mixed in 2.9 ml of cold tumour spheroid medium and seeded on low attachment plate (CORNING, cat no. 3471) at 37 °C in a 5% CO_2. Spheroids were harvested after 4 days for dissemination assays but were observed for up to 7 days in some experiments.

2.2 Fabrication technology of patterned platforms and collagen coating

Microfabrication technology was used to generate platforms with different topographies. SPR6112 positive photoresist was first patterned on a silicon (Si) substrate using photolithography. The Si substrate was etched with deep reactive ion etching to create a Si stamp with 15 μm deep grating patterns. Trichloro(1*H*,1*H*,2*H*,2*H*-perfluorooctyl)silane (FOTS, 97%, J&K Scientific) was coated on the Si stamp at 80 °C for 2 h, which acted as an anti-sticking hydrophobic layer with surface energy of 17 ± 1 mN m^{-1} and this was needed to release the platforms from the stamp when demolding. Polydimethylsiloxane (PDMS) prepolymer was mixed with curing agent (Dow Corning Sylgard 184 kit) in 10 : 1 (w/w) ratio and spin-coated onto the Si stamp at 3000 rpm for 1 min. The resulted 30 μm thick PDMS layer on the stamp was baked at 80 °C for 6 h and then demolded. The

prepared platform was attached to a 35 mm confocal dish and exposed to an oxygen (O_2) plasma with 20 sccm O_2 at 80 mTorr and 60 W RF power for 1 min to enhance the hydrophilicity with surface energy of 71 ± 3 mN m^{-1}. Collagen I (100 μg ml^{-1} in deionised water, Gibco) was added on the platform immediately after the O_2 plasma treatment to cover the entire platform. The sample was then kept at 18 °C for 1 h with ventilation. After collagen coating, excessive collagen was washed away gently using 1× phosphate saline buffer (PBS).

2.3 Tumour spheroid dissemination assay

NPC43 tumour spheroids were harvested at day 4 of 3D culture by gentle pipetting and transferred to the PDMS platforms. The spheroids were cultured in the absence of Matrigel. In some experiments, the spheroids were incubated with Hoechst 33342 (Thermofisher, cat no. 62249) at a final concentration of 1 μg ml^{-1} in culture medium for 30 min.

2.4 Confocal microscopy

The size of tumour spheroids, hence the cell number per spheroid, was highly heterogenous due to the random clustering of cells during seeding. In order to normalise the number of cells per spheroid in this study, only spheroids of diameters of 40–50 μm on the day of seeding were selected for subsequent analysis. Such normalisation would provide better analysis of the number of FAs protruding from the spheroids on different substrates. Coordinates of spheroids imaged on the first day were recorded so that the same spheroids were imaged in every time point.

2.5 Scanning electron microscopy

After seeding the spheroids on the platforms for 4 days, they were washed with 1× PBS and immersed in 4% paraformaldehyde for 15 min for fixation. To dehydrate the samples, the fixed spheroids were soaked in deionised water and a series of ethanol (30%, 50%, 70%, 80%, 90%, 95%, and 100%) for 5 min for each concentration. The samples were transitioned into a carbon dioxide environment using a critical point dryer (EM CPD300, Leica). A thin layer of gold was coated on the samples to prevent charging up of the sample. A scanning electron microscope (SEM, Hitachi SU5000) was then used to capture the images of NPC43 spheroids seeded on the platforms.

2.6 Immunofluorescence staining

At each time point, tumour spheroids were rinsed with 1× PBS (3 × 5 min) and then incubated with 4% paraformaldehyde (in PBS) at room temperature for 15 min. After washing in 1× PBS (2 × 10 min), the spheroids were permeabilised with 0.25% Triton-X100 (in PBS) at room temperature for 10 min and then washed with 1× PBS (2 × 10 min). After that, spheroids were blocked with 1% (w/v) bovine serum albumin (Sigma Aldrich) in PBST (0.01% Triton X100 in 1× PBS) at room temperature for one hour. The spheroids were then incubated with mouse anti-vinculin (Millipore, diluted 1 : 100 in PBST) for at 4 °C overnight. After washing in 1× PBST (2 × 10 min), the spheroids were incubated with Alexa 488-conjugated goat anti mouse (Invitrogen, 1 : 500 in PBST) for at room temperature in the dark for one hour. Then, spheroids were washed with 1× PBST (2 × 10 min). Finally, Hoechst 33342 (Thermofisher, cat no. 62249) was added to the spheroids at a concentration of 1 μg ml^{-1} and the mixture was incubated at room temperature in the dark for fifteen minutes. Then, spheroids were immersed in 1× PBS and imaged on a confocal microscope (Leica SPE).

2.7 Expression of EBV encoded genes

The expression of EBV genes was detected by qRT-PCR as described previously.[20] Briefly, total RNA samples were extracted using TRIzol reagent (Invitrogen) from NPC43 spheroids harvested after 4 days of cultures and from NPC43 cells cultured in 2D with ROCK inhibitor from the same parental plate. Reverse transcription and SuperScript First-Strand Synthesis System for RT-PCR (Invitrogen) were performed according to the manufacturer's protocols. The primers for EBV genes are reported.[20] The expression levels of these genes were normalised to GAPDH and the relative expression levels of genes of interest were determined by the $2^{-\Delta\Delta C_t}$ method.

2.8 Data analysis

The microscopy images captured in this project were analysed using NIH ImageJ (version 1.50i) installed with manual tracking plugin. Spheroids that contacted with other spheroids during the 4 day seeding period were excluded. To test the significant correlations, one-way analysis of variance (ANOVA) was used for comparison of the mean values of two or more groups. All the groups of data were labelled with the tick marks, and the results were shown as mean ± standard error of the mean. When $p > 0.05$, it indicated that the comparison test between the groups was not significant (NS). Tukey–Kramer method was used for *post hoc* test on groups with overall $p < 0.05$ to compare the difference between each pair of data.

3. Results

3.1 Establishment of nasopharyngeal spheroid culture

In this study, we investigated the impact of topographic cues on the migration characteristics of nasopharyngeal cancer cells from 3D spheroids. To achieve this, we used NPC43, a newly established patient-derived cell line.[20] NPC43 cells are shown to remain EBV positive after prolonged culture, a unique molecular hallmark of NPC, making this cell line a promising *in vitro* model for this cancer. For example, using this cell line, we have recently demonstrated that the formation of invadosomes in nasopharyngeal cancer cells was precisely regulated by the topography of the surrounding space,[4] suggesting that the invasiveness of nasopharyngeal cancer is highly dependent on the physical and mechanical information in the tumour microenvironment.

Despite these advantages, the behaviour of NPC43 cells in 3D culture have not been characterised. Here, we cultured NPC43 3D spheroids in ultra-low attachment plates with Matrigel. The use of Matrigel provided the NPC43 spheroids with

a biomimetic ECM.[29] Fig. 1a shows that NCP43 cells readily formed spherical aggregates after one day of culture. The size of the spheres gradually increased to an average of 100 μm on day 7 (Fig. 1c). Using a DNA-specific dye to label individual nuclei, we observed a 10-fold increase in cell number (equivalent to 3.3 doubling) in 7 days (Fig. 1b and c). The cell doubling time (about 2 day) was significantly shorter than that of NPC43 cells of similar passage number in 2D culture,[20] suggesting these cells proliferated more efficiently in a more physiologically relevant culture condition. EBV-encoded genes were still detectable in the spheroid (ESI Fig. S1†), with expression levels even higher than those in 2D culture, indicating that the NPC43 spheroid is a valid model for NPC.

Next, we asked whether NPC43 cells could migrate out of the 3D spheroids when seeded on a flat substratum. NPC43 spheroids collected after 4 days of 3D culture were transferred to a flat PDMS surface without Matrigel and further cultured for up to 4 days. While no significant cell spreading was observed on PDMS surface that was not coated with any ECM molecules, NPC43 spheroids disseminated efficiently on the surface coated with 100 μg ml^{-1} collagen I (Fig. 1d), in consistent with previous observations on the importance of ECM coating in tumour spheroid invasion assays.[30] NPC43 cells appeared to migrate collectively from the spheroids in a sheet-like manner, forming flat cellular protrusions on the leading edges. This migration characteristic is similar to that of other tumour spheroids.[31] As individual cells could not be distinguished in this collective migration, we stably expressed Lifeact-mCherry in NPC43 cells in order to aid the observation of the spreading front (Fig. 1d, arrowed). A previous study has shown that the expression of Lifeact-mCherry did not affect the proliferation and migration properties of NPC43 cells.[4]

3.2 Engineered surfaces for nasopharyngeal spheroid dissemination assay: theoretical considerations

Next, the spreading characteristics of NPC43 spheroids on PDMS platforms patterned with grating structures of different geometries were studied. To achieve this aim, we have designed a series of engineered substrates bearing a regular pattern of ridges (R) and trenches (T) (Fig. 2a). Three platforms, varied in ridge and trench widths, were fabricated: 40/10, 18/18, and 50/50 μm (R/T, Fig. 2b–d). The dimensions of the surface topographies formed by the ridges and trenches of the grating platforms were based on the NPC43 cell and spheroid sizes, and the number of grating edges they would contact when seeded on the platforms. The width of the trenches of 10, 18, and 50 μm was designed to be much narrower, similar, and larger than the typical size of a single NPC43 cell (15–20 μm). The depth of all the grating structures was 15 μm and it matched the typical size of an individual NPC43 cell. With such designs of surface topographies, the NPC43 spheroids and the subsequently protruding cells were exposed to different topographical microenvironment, as indicated by the number of vertical edges shown in Fig. 2e. Our previous work has shown that FA, known to be important in regulating cell migration,[32] are stabilised along the edges of engineered substrates with uneven surfaces.[5] Therefore, we hypothesize that the number of edges exposed to NPC43 spheroids may influence the dynamics of cell dissemination, possibly by providing larger surface area for cell adhesion. First, we considered the number of edges in contact to a NPC43 spheroid when it landed on a surface. Fig. 2e shows the possible scenarios when a NPC43 spheroid with a diameter of 50 μm (typical size of the spheroids harvested after 4–5 days of

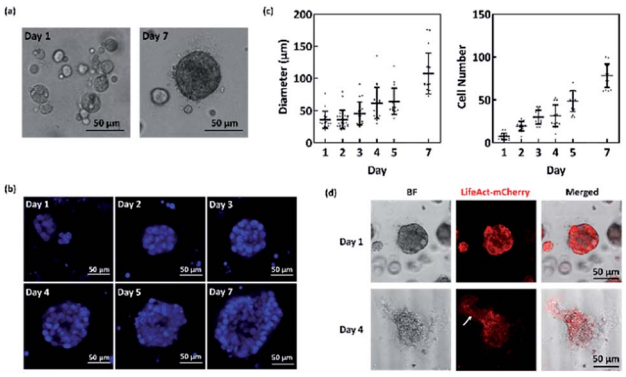

Fig. 1 (a) Brightfield images showing NPC43 cells cultured on low attachment plate with 2% Matrigel for 1 and 7 days (b) Hoechst-labeled nuclei in NPC43 spheroids after 1–7 days of culture. (c) Diameter and number of cells per spheroids of NPC43 spheroids after 1–7 days of culture. (d) NPC43 spheroids 1 and 4 days after transferred to collagen I-coated flat PDMS surface.

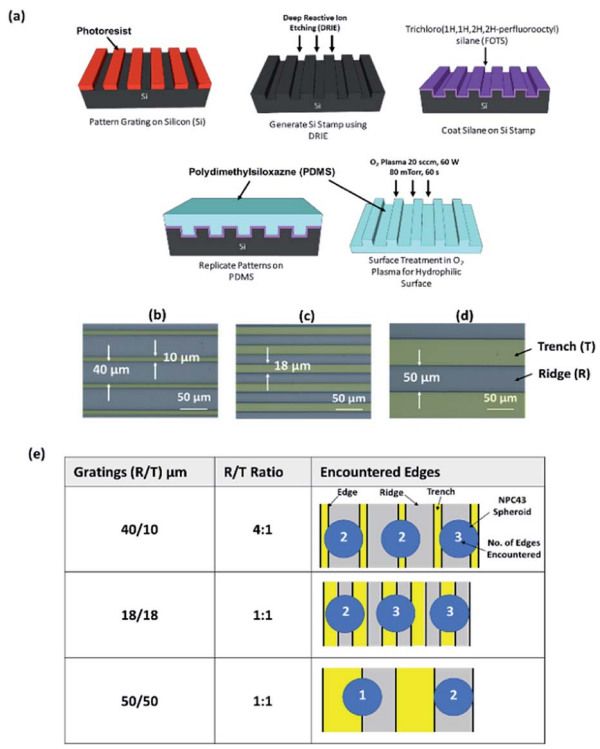

Fig. 2 (a) Fabrication technology of the PDMS platforms with grating structures. Micrographs of (b) 40/10 μm, (c) 18/18 μm, and (d) 50/50 μm (R/T) PDMS platforms with 15 μm deep grating platforms. (e) Schematic of NPC43 spheroids with size of 50 μm diameter seeded onto engineered grating platforms.

3D culture, Fig. 1b) was seeded on the different substrates used in this study. The spacing between the ridges and the trenches was designed to control the number of edges encountered by the protruding NPC43 cells. As the spacing between edges of the 18/18 μm (R/T) grating platforms were similar to the size of individual NPC43 cells, each NPC43 cell will likely to simultaneously contact to two edges when it migrates from the spheroid. However, although the 50/50 μm (R/T) grating platforms also consist of ridges and trenches in 1 : 1 ratio, the spacing of this pattern is more than double of NPC43 cell size, each protruding NPC43 cell could initially adhere to only one edge. The 40/10 μm (R/T) grating pattern was designed with 4 : 1 ratio between the width of the ridges and the trenches. As a result, the NPC43 cells had a higher chance to adhere to the ridge than the trench. Also, the confined space of the 10 μm wide trenches might restrict the access of NPC43 cells. Thus, using these three patterns, we aimed to study how NPC43 cells migrated when the spheroids were confronted with an uneven surface with different number of edges, in different dimensions relative to the size of individual spheroids.

3.3 NPC43 spheroids spreading on platforms with different topographies

Fig. 3 shows the ultrastructure of NPC43 spheroids 4 days after spreading on flat, 40/10, 18/18, and 50/50 μm PDMS surfaces coated with 100 μg ml^{-1} collagen I. In consistent with the brightfield morphology of NCP43 spheroids on flat surface (Fig. 1d), the SEM images show protrusion of a sheet-like structure from the spheroid body. For the results shown in Fig. 3, the area covering the entire sheet-like structure from spheroids on different platforms was measured and the significant difference among the groups of platforms was statistically analysed by ANOVA, and the difference between each pair of groups was verified by Tukey–Kramer *post hoc* test. Multiple comparisons between different groups were carried out and the 18/18 μm (R/T) grating platform showed significant effect on the NPC43 spheroid spreading area compared to the flat surface. NPC43 spheroids seeded on flat PDMS surface had the largest projected area of $26.7 \pm 8 \times 10^3$ μm^2, significantly ($^*p < 0.05$) larger than the spheroids on 18/18 μm (R/T) grating platforms, which had the smallest spreading area of $7.8 \pm 2 \times 10^3$ μm^2 among all platforms as shown in Fig. 3. The spreading area of spheroids on the other two grating platforms was also smaller than those on the flat surface, albeit with no statistical significance ($p > 0.05$). Hence, these data indicate that spheroid spreading, which may be related to the speed of the collective migration of cells from NPC43 spheroids, could be influenced by occurrence of the grating surface in the invaded area.

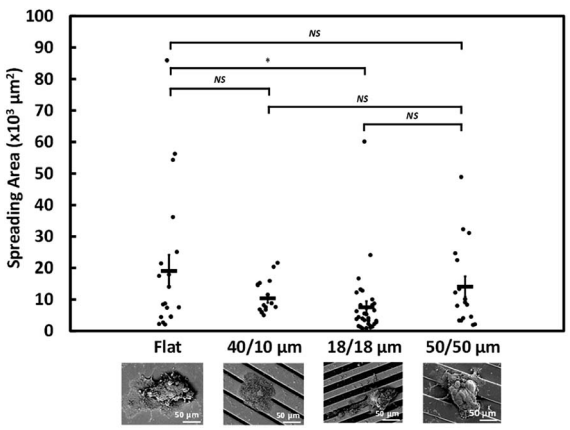

Fig. 3 Projected area of NPC43 spheroids obtained from SEMs after seeding on flat, 40/10, 18/18, and 50/50 μm (R/T) grating platforms for 4 days ($^*p < 0.05$, NS – not significant, one-way ANOVA with Tukey–Kramer test).

3.4 NPC43 spheroids elongated and aligned with grating orientation

On a flat surface, cancer cells migrate radially from tumour spheroids.[33] Our previous work has demonstrated that asymmetry of topographical patterns on cell culture substrate could influence the morphology and migration dynamics of cells cultured in a non-confluent condition.[7] To study the effects of topographical cues on the collective migration of cells from tumour spheroids, we seeded NPC43 spheroids on the platforms with flat surface, 40/10, 18/18, and 50/50 μm (R/T) grating platforms and investigated their spreading orientation during a 4 day period.

To observe the dynamics of cell spreading, we performed live cell imaging of NPC43 spheroids on different platforms over a period of 4 days (Fig. 4). To observe the dynamics of cell spreading, we performed live cell imaging of NPC43 spheroids on different platforms over a period of 4 days (Fig. 4). The time-lapse imaging experiments performed in this study contained only four time points, separated by 24 h intervals. This was because the spheroid dissemination process was relatively slow and continuous imaging would increase the risk of photo-damages. The leading edges of the spheroids were defined by the nucleus and cytoplasm of individual cells, indicated by Hoechst 33342 and Lifeact-mCherry fluorescence respectively. Representative confocal images confirmed our SEM observations (Fig. 4a) that NPC43 cells appeared to spread out more widely on the flat PDMS surface than on the three grating platforms. Interestingly, the spreading of NPC43 cells from the spheroids appeared to be asymmetrical on the grating surfaces. To quantitate the change of spheroid ellipsoidity during spreading, we measured the aspect ratio of individual spheroids, defined by the ratio between the major and the minor axis of the mCherry-labeled spheroid (Fig. 4b). The data represented in Fig. 4c shows the effect of surface topography on the directionality of cell spreading from tumour spheroids. The flat PDMS surface was used as the control. Spheroids in suspension before seeding on the platforms were also shown as day 0 for comparison. The statistical analysis shown in Fig. 4c were results of the one-way ANOVA with Tukey–Kramer test of the NPC43 spheroids among results obtained after day 1, 2, and 4 on different platforms. The results indicated that there was no significant difference for the aspect ratio of the NPC43 spheroids after 1, 2 and 4 culture days for flat surface, 40/10 μm and 50/50 μm (R/T) grating platforms. The aspect ratio of spheroids on flat surface remained unchanged, and close to one, over the 4 day period, in consistent with the radial spreading of other

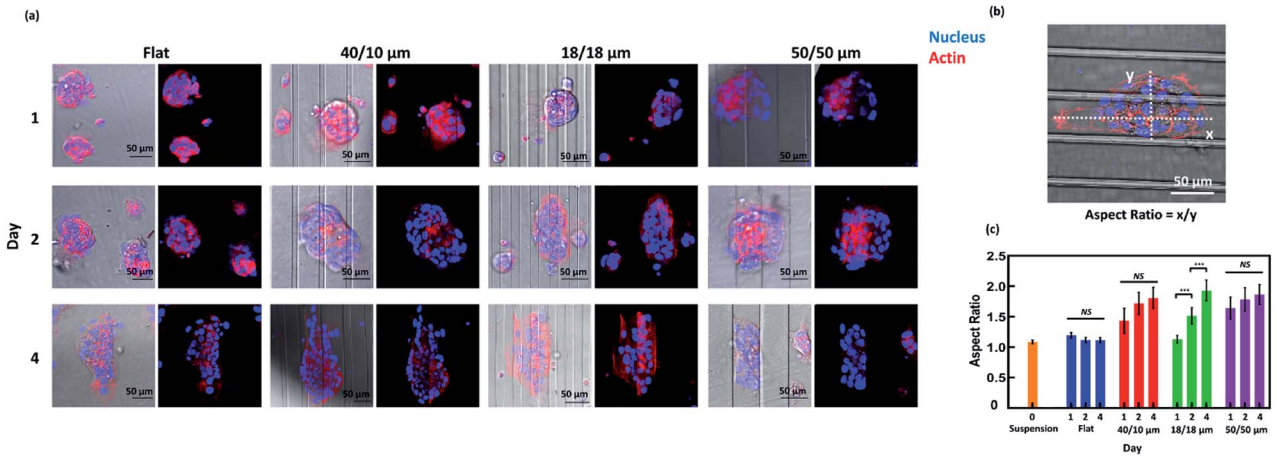

Fig. 4 (a) Morphology of NPC43 spheroids cultured on flat, 40/10, 18/18, and 50/50 μm (R/T) grating platforms for 1–4 days. (b) Definition of the aspect ratio of NPC43 spheroids. (c) Aspect ratios of NPC43 spheroids on the four PDMS platforms after 1–4 days of culture days (***$p < 0.001$, NS – not significant, one-way ANOVA with Tukey–Kramer test).

cancer cells previously observed in spheroid invasion assays. However, the NPC43 spheroids elongated on all grating platforms. Spheroids on the 50/50 μm grating adopted on ellipsoid morphology (aspect ratio = 1.6) as early as 1 day after seeding. Spheroids on the 18/18 μm grating were initially symmetrical (aspect ratio ~1) on day 1, but rapidly elongated over the course of 4 days, until their aspect ratios (~1.9) were comparable to the spheroids on 50/50 μm grating. The aspect ratio of the spheroids on 40/10 μm grating was comparatively lower (1.5–1.8) but was still higher than that on flat surface (Fig. 4c).

As Lifeact-mCherry fluorescence did not necessarily capture the outline of the thin sheet-like structures protruding from the spheroids, we characterised the morphology of NPC43 spheroids on day 4 of the dissemination assay by SEM (Fig. 5a). One-way ANOVA followed by Tukey–Kramer method for *post hoc* test were applied to analyse the aspect ratio and spreading orientation of NPC43 spheroids on patterned surfaces obtained from SEM was shown in Fig. 5b and c. Multiple analysis were carried out to compare the statistically significant difference between each two groups of platforms. Multiple analysis were carried out to compare the statistically significant difference between each two groups of platforms. Fig. 5b shows that NPC43 spheroids on flat PDMS surface remained relatively symmetrical after 4 days of spreading, with an average aspect ratio of 1.46. The aspect ratio of spheroids on 40/10 μm (R/T) grating platforms was close to that on the flat PDMS platforms (1.5). NPC43 spheroids on 18/18 and 50/50 μm (R/T) grating platforms elongated to an aspect ratio of 2.0 and 2.1 respectively. Thus, our ultrastructural data were consistent with the data from confocal imaging, underpinning the pronounced effect of 18/18 and 50/50 μm (R/T) grating platforms on the cell spreading. Interestingly, our SEM images (Fig. 5a) indicated that although the spreading of the sheet-like protrusion on the grating platforms appeared ellipsoid, the core of the spheroid remained relatively symmetrical. This suggests that the surface topography affects the directionality of the outspreading cells and not the general shape of the tumour spheroid. To better characterise the dissemination behaviour, the orientation representing the directionality of collective NPC43 cells released from the NPC43 spheroids was calculated by measuring the absolute deviation angle between the grating orientation and the spheroid major axis as shown in Fig. 5a. If the spreading of NPC43 cells was completely aligned with the main axis of the grating, the measured deviation angle would be 0°. As shown in Fig. 5c, the spreading orientation of NPC43 spheroids on 40/10 μm grating structures had a deviation angle of 19.5°. However, NPC43 spheroids spread along the grating orientation when seeded on the 18/18 and 50/50 μm (R/T) grating platforms with a similar deviation angle of 10.5° and 10.0°, respectively. Taken together,

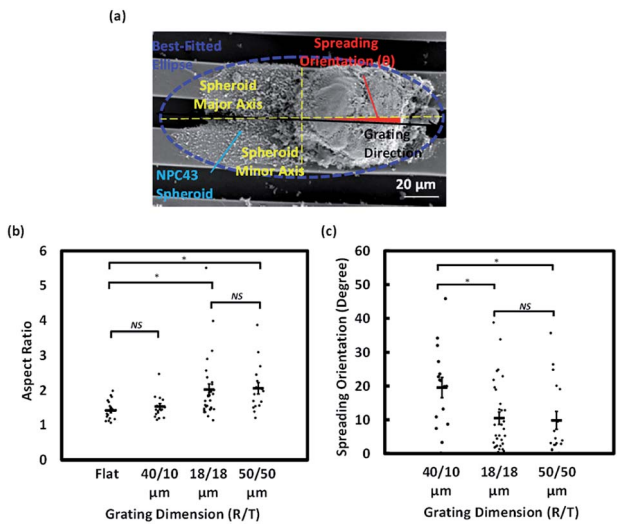

Fig. 5 Aspect ratio and spreading orientation of NPC43 spheroids on patterned surfaces (*$p < 0.05$, NS – not significant, one-way ANOVA with Tukey–Kramer test). (a) Micrograph of NPC43 spheroids on 18/18 μm (R/T) grating platforms and definitions of spreading statistics. (b) Aspect ratio and (c) spreading orientation of NPC43 spheroids on flat, 40/10, 18/18, and 50/50 μm (R/T) grating platforms after 4 day seeding period.

these data indicate that the spreading of NPC43 cells from spheroids on the 18/18 and 50/50 μm (R/T) platforms was not only more asymmetrical but also more aligned to the grating platforms. Hence, compared to the 40/10 μm (R/T) grating platforms, these two platforms appeared to provide better guidance to NPC43 cell spreading from spheroids.

3.5 Effect of grating topography on FAs on leading edges protruding from NPC43 spheroids

Filopodia are known to be important to cancer cell adhesion, migration and invasion.[34] We next investigated the localisation and abundance of FAs, detected by vinculin immunofluorescence, in the NPC43 spheroids cultured on flat surface, 40/10, 18/18, and 50/50 μm (R/T) grating platforms (Fig. 6). As NPC43 cells did not spread out from the spheroids as individual amoeboid cells, we could not identify the FAs of each protruding cell. Rather, we counted all the FAs on the leading edge of the entire spheroid. Fig. 6b shows the total number of FAs counted on spheroids of similar initial size (40–50 μm) after 4 days of culture. The number of FAs per spheroid was analysed by ANOVA on different patterned platforms and the results were shown in Fig. 6b. Approximately 80 FAs were detected in spheroids on flat PDMS surface, with a higher number (109 ± 26 FAs) found in spheroids on the 50/50 μm (R/T) grating platforms. Meanwhile, the number of FAs on the 40/10 and 18/18 μm (R/T) grating platforms was lower (39 ± 4 and 48 ± 18 FAs, respectively), but the difference was not statistically significant. Next, we asked whether the FAs of the protruding NPC43 cells were preferentially formed on the ridge or the trench of the grating platforms. To achieve this, we scored the number of FAs on two confocal planes separated by 15 μm, focusing on the ridge and the trench of each platform respectively. As shown in Fig. 6c, there were consistently more FAs on the ridge region than the trench of all three grating platforms. There were almost no detectable FA in the trench of 40/10 μm (R/T) grating, suggesting that the 10 μm trench of this surface was too narrow for NPC43 cells to enter. The number of FAs detected in the trenches was apparently proportionally the trench width, as there was more FAs in the 50 μm wide trenches than in the 18 μm wide ones. The restriction of FA formation in the trenches, especially in the 18/18 and 40/10 μm (R/T) grating platforms was probably the cause of the lower FA number of spheroids on these platforms than on flat surface. However, even for the 50/50 μm (R/T) grating, where both the ridges and the trenches should be equally accessible, we still detected significantly more FAs on the ridges than in the trenches. These data suggest a preference to the ridge for the formation of FAs by NPC43 cells spreading from spheroids.

4. Discussion

The dissemination of tumour spheroids on cell culture surfaces is a simple and powerful *in vitro* model for the study of cancer metastasis.[35] In these assays, cancer cells invade the surroundings from 3D cultured clusters through the interaction with ECM proteins. Here, we investigated the roles of topographical information of the culture microenvironment on the dynamics of nasopharyngeal tumour spheroid dissemination by using a combination of imaging techniques. As far as we know, this study is the first of its kind, highlighting the feasibility and convenience of using microfabricated engineered surfaces to study tumour metastasis *in vitro*. In this study, we designed and fabricated three types of platforms based around the central theme of grating. Grated surfaces of various dimensions have consistently been shown to affect migration behaviours of cancer cells depending on their metastatic properties.[7,12,36–38] In particular, our

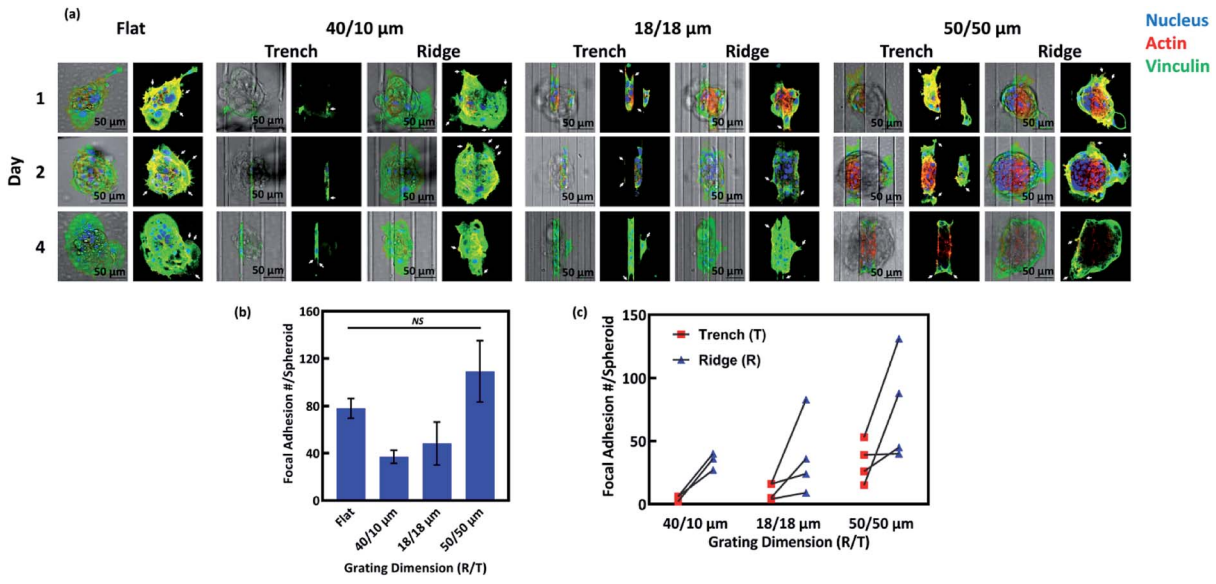

Fig. 6 (a) Confocal images of representative NPC43 spheroids on flat, 40/10, 18/18, and 50/50 μm (R/T) grating platforms after 1–4 days of culture. (b) Average number of FAs detected in a NPC43 spheroid on the four PDMS platforms on day 4 (NS – not significant, one-way ANOVA). (c) Number of FAs detected on the ridge (triangles) and the trench (squares). Data from the same spheroid are linked by black lines.

team has shown that the asymmetry and dimension of the patterns significantly influences the migration speed and directionality of cancer cells.[4–7] However, all these previous studies were performed on non-confluent 2D cultured, independently migrating cells. Here, as a proof of concept, we exposed NPC43 tumour spheroids to grating platforms with different spacing regularities and dimensions, in order to observe how the number and types of edges may affect tumour dissemination.

Our data indicate that, when other conditions such as ECM coating and substrate elasticity, were normalised, NPC43 spheroids generally spread less efficiently and more asymmetrical on grated surfaces than a flat surface. We observed that the spreading of NPC43 cells was the more restricted on 18/18 μm than on the 50/50 μm (R/T) grating platforms, suggesting the density of edges encountered by the disseminating tumour spheroids may influence spreading efficiency. In consistent with this hypothesis, despite the NPC43 spheroids encountering two to three grating edges on both the 18/18 and 40/10 μm (R/T) grating platforms, there is a higher probability that a NPC43 spheroid would encounter three edges on the 18/18 μm (R/T) grating platforms platform than the 40/10 μm (R/T) grating platforms. This result suggests an inverse correlation between the density of grating edges and the spreading area of the NPC43 spheroids. The higher number of grating edges could restrict the NPC43 spheroids from spreading out thus leading to a smaller projected area of the spheroids.

We observed that NPC43 cells spread asymmetrically on grated surfaces, leading to the formation of ellipsoid leading fronts around the spheroids. For example, both fluorescent and scanning electron microscopy showed that NPC43 spheroids on 18/18 and 50/50 μm (R/T) grating platforms elongated along grating structures with an aspect ratio of close to 2, significantly deviated from that on the flat surface. It is suggested that the edges of the 18/18 and 50/50 μm (R/T) grating platforms provided additional surface area for NPC43 spheroid and cell attachment, guiding the outgrowing NPC43 cells to migrate along the grating edges. This asymmetrical migration may cause the NPC43 spheroids to form an elliptical shape after the 4 day seeding period on these grating platforms. Interestingly, spheroids cultured on 40/10 μm (R/T) grating platforms appeared to offer the least guidance: NPC43 spheroids spread on this platform with an aspect ratio of 1.5, similar to that on the flat PDMS surface. We interpret this as an indication that NPC43 cells from spheroids on the 40/10 μm (R/T) grating platforms were less likely to squeeze into the confined 10 μm wide trenches. As a result, the spheroids tended to spread out on the relatively more spacious 40 μm wide ridges in random orientation as if they were a flat surface. In consistent with this interpretation, almost no FA was detected in the trenches of the 40/10 μm (R/T) grating platforms, suggesting that these confined spaces were inaccessible to the spreading NPC43 cells.

Our previous work has demonstrated single cell migration behaviours of NP460 cells on 5/5, 18/18, and 50/50 μm (R/T) grating platforms with 1 μm depth. The results showed that the cells on 18/18 and 50/50 μm (R/T) grating platforms migrated with similar speed but 18/18 μm (R/T) grating structures guided the cells to migrate along the grating orientation with better alignment than 50/50 μm (R/T) grating platforms.[4] The directionality and motility of MC3T3-E1 cells on PDMS engineered platforms were investigated and the cells were found to elongate along the main axis of the guiding patterns while they would spread randomly on flat surface.[6] In addition, NPC43 cells were found to elongate more with better alignment to the grating orientation on 5/5 μm (R/T) grating platforms with deeper trenches.[4] Similar to MC3T3-E1 cells, NPC43 cells extended filopodia in all directions without following the main axis of the 100 nm deep grating platforms,[4] as the shallow pattern was similar to a flat surface. In this project, NPC43 spheroids were found to elongate along the orientation of 40/10, 18/18, and 50/50 μm (R/T) grating platforms. When comparing the aspect ratio and spreading orientation of NPC43 spheroids under SEM after seeding on the platforms for four days, the spheroids showed similar behaviors of larger aspect ratio and better alignment on the 18/18 and 50/50 μm (R/T) grating platforms. However, single NP460 cell migration study showed 18/18 μm (R/T) grating platforms provided better guidance than 50/50 μm grating platforms[4] due to enhanced topographical cues for the single cells with size close to 18 μm. For NPC43 spheroids, the 18/18 and 50/50 μm (R/T) grating platforms provided similar guiding effects since the size of the NPC43 spheroids was similar to the 50/50 μm wide ridges and trenches. Therefore, the guiding capability of a platform would be affected by the size of a spheroid. As spheroids elongated on grating structures, individual NPC43 cell could release from the spheroids with different migration speed depending on the position of each cell in the spheroids. It will be useful to monitor the migration speed of NPC43 cells moving out of the spheroids in future study.

NPC43 spheroids appeared to navigate differently on different part of the grating. Vinculin staining indicated that mature FAs were more preferentially formed on the ridges than in the trenches. It is possible the ridges, as the more elevated surface of the platforms, represented the first point of contact when the spheroids were seeded, and it might take more time for the NPC43 cells to adhere to the trenches. No FA was able to form in the trenches of the 40/10 μm (R/T) platform (Fig. 6c), suggesting that trenches narrower than the size of NPC43 cells are inaccessible to the spreading cells. It is interesting to notice that the dimension of the trenches appears to affect the number of FAs on the ridges: NPC43 spheroids expressed on average ~60 FAs on the 50 μm ridges with 50 μm wide trenches, but only ~20 on the ridges of similar size (40 μm) when the trenches were 10 μm wide. As the number of FAs is associated with the speed of spheroid dissemination,[22,39] the lower number of FAs on the 40/10 μm (R/T) platform compared to other surfaces (Fig. 6b) probably explains the slower cell spreading rate observed on this platform (Fig. 3). Future investigations will be focused on how the localised exposure of a tumour spheroid to microenvironmental topography might affect molecular pathways that regulate cytoskeletal organisation and dynamics.

5. Conclusions

Taken together, our results demonstrate that tumour spheroids exhibited different spreading characteristics on different microenvironment. The experimental approach pioneered in this project can be extended to study the effect of other types of topographical signals on tumour dissemination. The

directional spreading of cancer cells from spheroids can also be utilised to design microsystems that can guide and capture metastatic cells. We believe this work represents an important step towards the introduction of more physiological and biomimetic environment for *in vitro* 3D cultured cell studies.

Conflicts of interest

There are no conflicts to declare.

Acknowledgements

We gratefully acknowledge Professors S. W. Tsao and C. M. Tsang from the School of Biomedical Science, the University of Hong Kong for providing the cell line studied in this project. We greatly appreciate the technical support from the staff at Centre for Biosystems, Neuroscience, and Nanotechnology (CBNN), Optoelectronics Laboratory, and Department of Chemistry. The editorial and technical assistance from Mr S. M. Tang are acknowledged. This work was supported by the CBNN of City University of Hong Kong [9360148, 9380062], and the University Grants Council of Hong Kong [GRF Projects: 11247716, 11218017, 11213018, 11212519, and CRF project: C1013-15G].

References

1 P. S. Steeg, *Nat. Rev. Cancer*, 2016, **16**, 201–218.
2 V. Mittal, *Annu. Rev. Phytopathol.*, 2018, **13**, 395–412.
3 A. M. Alizadeh, S. Shiri and S. Farsinejad, *Tumor Biol*, 2014, **35**, 8483–8523.
4 C. M. Tsang, Z. Y. Liu, W. Zhang, C. You, G. E. Jones, S. W. Tsao and S. W. Pang, *Acta Biomater.*, 2020, **101**, 168–182.
5 Q. Y. Tang, W. X. Qian, Y. H. Xu, S. Gopalakrishnan, J. Q. Wang, Y. W. Lam and S. W. Pang, *J. Biomed. Mater. Res., Part A*, 2015, **103**, 2383–2393.
6 Q. Y. Tang, W. Y. Tong, J. Shi, P. Shi, Y. W. Lam and S. W. Pang, *Biofabrication*, 2014, **6**, 015011.
7 S. F. Zhou, S. Gopalakrishnan, Y. H. Xu, S. K. Y. To, A. S. T. Wong, S. W. Pang and Y. W. Lam, *Biomed. Mater.*, 2017, **12**, 055001.
8 A. Ray, O. Lee, Z. Win, R. M. Edwards, P. W. Alford, D. H. Kim and P. P. Provenzano, *Nat. Commun.*, 2017, **8**, 14923.
9 A. S. Nunes, A. S. Barros, E. C. Costa, A. F. Moreira and I. J. Correia, *Biotechnol. Bioeng.*, 2019, **116**, 206–226.
10 C. D. Paul, P. Mistriotis and K. Konstantopoulos, *Nat. Rev. Cancer*, 2017, **17**, 131–140.
11 E. D. Tabdanov, V. V. Puram, Z. Win, A. Alamgir, P. W. Alford and P. P. Provenzano, *Nat. Commun.*, 2018, **9**, 4891.
12 K. Kushiro, T. Yaginuma, A. Ryo and M. Takai, *Sci. Rep.*, 2017, **7**, 4244.
13 S. Raghavan, P. Mehta, E. N. Horst, M. R. Ward, K. R. Rowley and G. Mehta, *Oncotarget*, 2016, **7**, 16948–16961.
14 M. Vinci, S. Gowan, F. Boxall, L. Patterson, M. Zimmermann, W. Court, C. Lomas, M. Mendiola, D. Hardisson and S. A. Eccles, *BMC Biol.*, 2012, **10**, 29.
15 J. Song, J. H. Shawky, Y. Kim, M. Hazar, P. R. LeDuc, M. Sitti and L. A. Davidson, *Biomaterials*, 2015, **58**, 1–9.
16 V. Brekhman and G. Neufeld, *BMC Cancer*, 2009, **9**, 415.
17 G. Benton, H. K. Kleinman, J. George and I. Arnaoutova, *Int. J. Cancer*, 2011, **128**, 1751–1757.
18 E. I. Deryugina and M. A. Bourdon, *J. Cell Sci.*, 1996, **109**, 643–652.
19 J. Tsang, V. H. Lee and D. L. Kwong, *Oral Oncol.*, 2014, **50**, 798–801.
20 W. Lin, Y. L. Yip, L. Jia, W. Deng, H. Zheng, W. Dai, J. M. Y. Ko, K. W. Lo, G. T. Y. Chung, K. Y. Yip, S. D. Lee, J. S. Kwan, J. Zhang, T. Liu, J. Y. Chan, D. L. Kwong, V. H. Lee, J. M. Nicholls, P. Busson, X. Liu, A. K. S. Chiang, K. F. Hui, H. Kwok, S. T. Cheung, Y. C. Cheung, C. K. Chan, B. Li, A. L. Cheung, P. M. Hau, Y. Zhou, C. M. Tsang, J. Middeldorp, H. Chen, M. L. Lung and S. W. Tsao, *Nat. Commun.*, 2018, **9**, 4663.
21 O. Ilina, G. J. Bakker, A. Vasaturo, R. M. Hofmann and P. Friedl, *Phys. Biol.*, 2011, **8**, 015010.
22 A. J. McKenzie, S. R. Hicks, K. V. Svec, H. Naughton, Z. L. Edmunds and A. K. Howe, *Sci. Rep.*, 2018, **8**, 7228.
23 D. Hanahan and R. A. Weinberg, *Cell*, 2000, **100**, 57–70.
24 J. S. Lowe and P. G. Anderson, in *Stevens & Lowe's Human Histology*, ed. J. S. Lowe and P. G. Anderson, Mosby, Philadelphia, 4th edn, 2015, pp. 37–54, DOI: 10.1016/B978-0-7234-3502-0.00003-6.
25 C. De Pascalis and S. Etienne-Manneville, *Mol. Biol. Cell*, 2017, **28**, 1833–1846.
26 A. W. Lee, W. T. Ng, Y. H. Chan, H. Sze, C. Chan and T. H. Lam, *Radiother. Oncol.*, 2012, **104**, 272–278.
27 J. R. Harkema, S. A. Carey and J. G. Wagner, *Toxicol. Pathol.*, 2006, **34**, 252–269.
28 P. A. Smith, D. Merritt, L. Barr and D. A. Thorley-Lawson, *Genes Cancer*, 2011, **2**, 1023–1033.
29 H. K. Kleinman and G. R. Martin, *Semin. Cancer Biol.*, 2005, **15**, 378–386.
30 M. Zimmermann, C. Box and S. A. Eccles, *Methods Mol. Biol.*, 2013, **986**, 227–252.
31 M. J. Ziperstein, A. Guzman and L. J. Kaufman, *PLoS One*, 2015, **10**, e0139523.
32 S. I. Fraley, Y. Feng, R. Krishnamurthy, D. H. Kim, A. Celedon, G. D. Longmore and D. Wirtz, *Nat. Cell Biol.*, 2010, **12**, 598–604.
33 K. J. Cheung, E. Gabrielson, Z. Werb and A. J. Ewald, *Cell*, 2013, **155**, 1639–1651.
34 G. Jacquemet, H. Hamidi and J. Ivaska, *Curr. Opin. Cell Biol.*, 2015, **36**, 23–31.
35 N. Kramer, A. Walzl, C. Unger, M. Rosner, G. Krupitza, M. Hengstschlager and H. Dolznig, *Mutat. Res.*, 2013, **752**, 10–24.
36 C. Rianna and M. Radmacher, *Nanoscale*, 2017, **9**, 11222–11230.
37 R. Rapier, J. Huq, R. Vishnubhotla, M. Bulic, C. M. Perrault, V. Metlushko, M. Cho, R. T. Tay and S. C. Glover, *Cancer Cell Int.*, 2010, **10**, 24.
38 T. Tzvetkova-Chevolleau, A. Stephanou, D. Fuard, J. Ohayon, P. Schiavone and P. Tracqui, *Biomaterials*, 2008, **29**, 1541–1551.
39 K. E. Sloan, J. K. Stewart, A. F. Treloar, R. T. Matthews and D. G. Jay, *Cancer Res.*, 2005, **65**, 10930–10937.